An Experimental Study of the Effect of Turbulent Mixing on the Selectivity of Competing Reactions

An experimental study of the effect of turbulent mixing on the selectivity of a parallel-consecutive reaction system ($A + B \rightarrow R$; $R + B \rightarrow S$) has been carried out in an unmixed feedstream (multijet) tubular reactor. Fluid mechanical characterization of the reactor by pulsed ultrasound Doppler velocimetry reveals that the mean and rms velocity fields are nearly constant over eight-ninths of the reactor length. Axial profiles of mean product concentration (R and S) have been measured spectrophotometrically with a fiber-optic probe under constant hydrodynamic conditions but with variable feed concentration conditions. The concentration profiles (particularly the S profile) show very large deviations from the perfect mixing (classical plug flow reactor) limit. These data provide a good basis for discriminating among the many models of mixing and reaction available in the literature. This is demonstrated with two examples: the four-environment model, which fits the data well, and the interaction by exchange with the mean model, which does not.

R. V. Mehta, J. M. Tarbell
Department of Chemical Engineering
Pennsylvania State University
University Park, PA 16802

Introduction

A proper understanding of turbulent mixing in chemical reactors is of vital importance in many industrial applications. Liquid phase mixing plays a critical role in precipitation processes where the shape and size of relatively insoluble precipitate particles can be significantly altered by changing the local mixing environment near the feed port (Garside, 1985). Similarly, the degree of mixing in the reactor strongly influences the initiator consumption in some commercial polymerization reactors (van der Molen et al., 1982). Turbulent mixing is also recognized as a key factor affecting the overall performance of a combustor, both in terms of fuel efficiency and formation of pollutants (Pratt, 1976).

The study of turbulent mixing with fast chemical reactions has resulted in the proposition of a large number of plausible theoretical models, and several review articles are available (Hill, 1979; Brodkey, 1981; Patterson, 1981; Villermaux, 1983;, Chang et al., 1986; Tarbell and Mehta, 1986). The models may be classified as either direct turbulence models or mechanistic models. The direct turbulence models are derived from the Navier-Stokes and component continuity equations and involve closure approximations (Patterson, 1979, 1981; Brodkey and Lewalle, 1985). The mechanistic models are not based on momentum and continuity equations but, rather, invoke idealized mechanisms of micromixing often involving the interdiffusion of inhomogeneous slabs or the intermixing of segregated environments at some prescribed rate (Villermaux; 1983, Tarbell and Mehta, 1986). They do not involve closure approximations. The mechanistic models are attractive because of their simplicity and modest computational demands, but the direct turbulence models offer the possibility of more general applicability. It should be noted that a relationship between the mechanistic and direct turbulence models has been demonstrated for five mechanistic models (Tarbell and Mehta, 1986; Chang et al., 1986).

The availability of so many mixing models naturally raises the question of discrimination: can they all be used equally well in design, analysis, and scale-up of reactors? The conclusion reached by Villermaux (1983) in a review paper was that most mechanistic models are approximately equivalent. Li and Toor (1986) concluded that four different mixing models compared equally well with their experimental data on the selectivity of a series-parallel reaction system (Bourne et al., 1981) in a tubular reactor. On the other hand, Chang et al. (1986), using numerical simulation of the same reaction system, found that under

certain conditions five models which give equivalent predictions for single reactions would predict very different selectivities for competing reactions. The numerical simulations indicated that significant differences in selectivity prediction would arise whenever the turbulent micromixing time scale in a tubular reactor was comparable to or larger than the intrinsic time scale of the slower reaction. Chang et al. concluded that experimental data for the series-parallel reaction scheme in a tubular reactor having a mixing time comparable to the intrinsic time scale of the slower reaction is required for unambiguous model discrimination. The purpose of this paper is to report such experimental data and to provide a preliminary evaluation of mixing models based on the new data.

The azo coupling of 1-naphthol (A) with diazotised sulfanilic acid (B) in dilute, aqueous, alkaline buffered solution at room temperature was chosen for experiments. The reaction is schematically represented by

$$A + B \xrightarrow{k_1} R$$

$$R + B \xrightarrow{k_2} S \qquad (1)$$

and was first proposed by Bourne et al. (1981) for use in mixing studies. It also has the fastest kinetics at room temperature among many candidate series-parallel reactions listed by Bourne (1982). Since the reaction products R (monoazo dye) and S (diazo dye) absorb visible light, their concentration can be measured by absorption spectrophotometry.

The instrinsic time scale of the primary coupling reaction at typical operating concentrations ($\overline{C_{BO}} = 0.3$ mol/m^3) is about 0.5 ms and that of the secondary coupling reaction is about 1 s (Chang et al., 1986). Hence, in the present work an unmixed feedstream tubular reactor was designed to have a micromixing time scale on the order of 1 s. To help clarify the interpretation of experimental turbulent reaction data, the reaction flow field was characterized by turbulence measurements based on a pulsed ultrasound-Doppler velocimeter. The turbulence measurements were also useful in estimating the micromixing time scale.

Experiments

General description

A diagram of the flow system used in this study is shown in Figure 1. Alkaline buffered 1-naphthol solution (A) was pumped by a sealless magnetic drive centrifugal pump through a rotameter to a flow distributor. Passage of the flow through the distributor was expected to develop a nearly flat velocity profile, and subsequent passage through a contraction nozzle provided further reduction in the level of existing turbulence. The flow then passed through a "hairbrush" multineedle injector, Figure 2, a turbulence generator screen, and entered the tubular reactor. Diazotized sulfanilic acid solution (B) was pumped into the plenum chamber of the injector by a laboratory metering pump. The acid solution then entered the alkaline main flow through the injector needles in the form of isokinetic axial jets. Isokinetic injection required a large difference between the flow rates of the two reactant streams. As a result, the acid solution was proportionately more concentrated to meet the requirements of overall feed stoichiometry. The injector was designed to provide a uniform coarse scale distribution of reactants over the reactor cross section while permitting minimal micromixing and hence, little reaction.

Most of the flow loop piping was made from PVC: 2.54 cm ID for the main flow, and 0.64 cm ID for the acid stream. The rota-

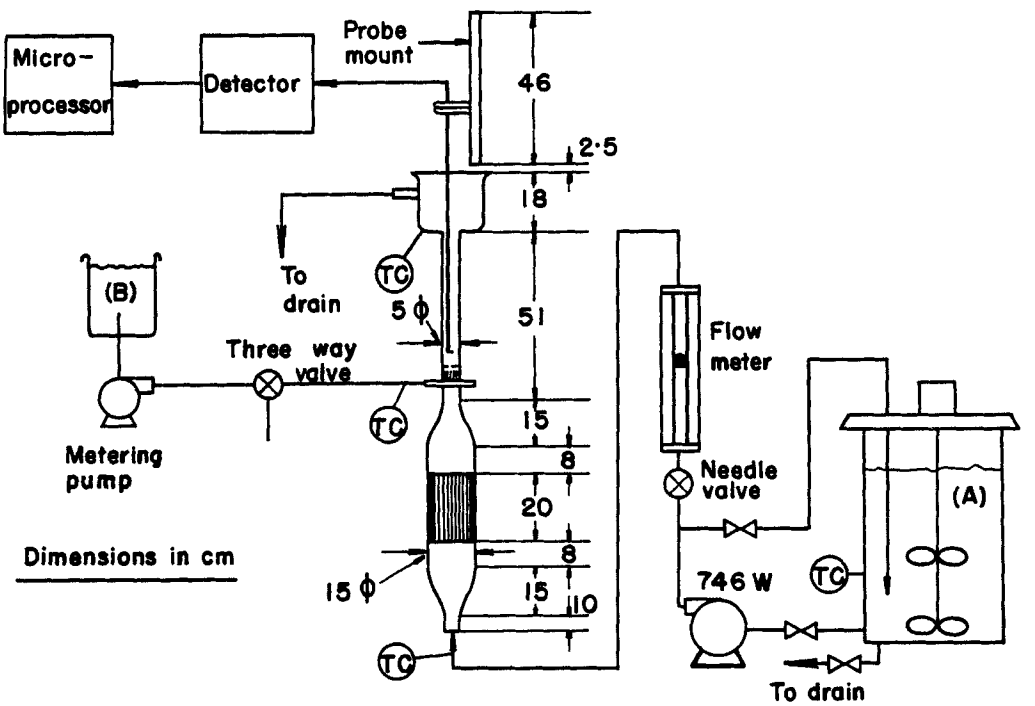

Figure 1. Experimental system.
All dimensions in cm

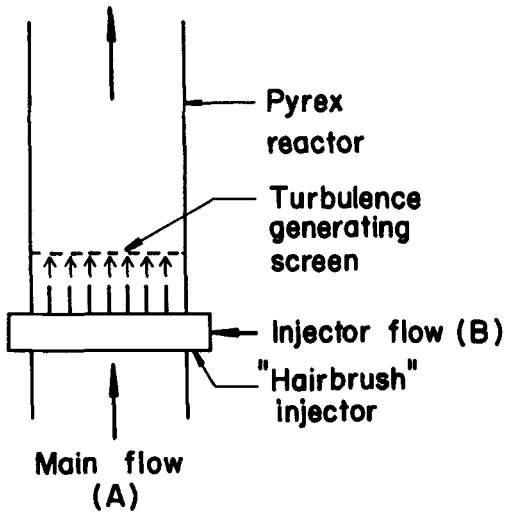

Figure 2. Injector system.

meter and needle valve were made from stainless steel. The tubular reactor was simply a 0.45 m length of 5.08 cm ID Pyrex pipe that terminated in a stainless steel overflow chamber. A honeycomb type flow distributor made from plastic soda straws (6 mm ID) whose cells had a large length-to-diameter ratio ($L/D = 33$) was employed. The straws were packed into a 15 cm ID Pyrex pipe and held in place by silicon rubber applied on each straw. The estimated solidity (fraction of pipe area not open to the flow) of the honeycomb was 0.33. Thus, the solidity was kept well below a critical value of 0.43 prescribed by Tan Atichat et al. (1982), and no central jet formation was expected. A 0.5 dia. long settling chamber followed the honeycomb to allow the mean velocity profiles emanating from individual straws to merge and settle to a uniform profile. The contraction nozzle led to an area reduction by a factor of nine, which conformed to standard water tunnel practice. The nozzle was about one upstream diameter long and tapered very gradually at the downstream end. The "hairbrush" injector was a duplicate of the one used by Keeler (1964). It consisted of a matrix of 18 gauge stainless steel hypodermic needles arranged on a 0.8 cm square lattice. The circumscribing plenum chamber (10 cm OD, 5 cm ID) distributed the B stream among seven parallel tubes (3.18 mm ID), which in turn distributed the flow among 37 needles. The plenum chamber was constructed from brass and its interior was coated with protective varnish to prevent any reaction between the B stream and the injector wall. The turbulence generator screens were ordinary stainless steel wire mesh screens. Three screens, with the specifications listed in Table 1, were used in the present work. A screen was placed either 0.7 cm upstream of 0.7 cm downstream of the injector so as to vary mixing conditions in the reactor. The probe mount was a 50 cm long vernier slide mounted on a grooved stainless steel plate which permitted three-dimensional movement of the probes. The axial positioning accuracy of the probe mount was 0.25 mm. The same probe mount was used to hold the acoustic transducer in PUDV measurements and the fiber-optic probe in mixing-reaction studies. Further details of the experiments can be found in Mehta (1985).

Table 1. Screen Specifications

	Screen		
	M_1	M_2	M_3
Solidity, S^*	0.43	0.39	0.60
Wire diam., d, mm	1.01	0.46	0.31
Mesh length, M, mm	4.24	2.12	0.85
Mesh ratio, $M/2$	4.22	4.63	2.73

*$S = 1 - (M - d)^2/M^2$

Flow field characterization

Flow field characterization involved measurement of the mean and root mean square (RMS) velocities at several positions in the reactor. These experiments were conducted separately from the mixing-reaction studies but at the same pipe Reynolds number of 3,400. A pulsed ultrasonic Doppler velocimeter (PUDV) was used for the measurements.

The PUDV operates on the Doppler principle. When sound waves are reflected off a moving particle in the flow, there is a frequency shift. This Doppler shift, Δf_d, is related to the velocity u of the moving particle in the following manner

$$\Delta f_d = \frac{2uf_o \cos\theta}{u_s} \tag{2}$$

where u_s is the speed of sound in the flow medium, θ is the acute angle between the direction of the sound wave and the velocity vector, and f_o is the frequency of the incident sound waves. If the particle follows the local flow closely then measurement of the Doppler shift provides a measure of the local velocity. Further details of the operation of the PUDV are provided by Jorgensen et al. (1973), and its use in measurement of fluid turbulence is discussed by Garibini et al. (1982) and Tarbell et al. (1986).

In the present work, ordinary tap water, with its fine mist of air bubbles, was used as the working fluid. The air bubbles served as the scattering particles. The mean bubble diameter, based on Stoke's law, was estimated to be 60 μm and the mean bubble rise velocity was about 3% of the mean flow velocity in the reactor. Therefore, the bubbles were expected to follow the turbulent flow field well. The acoustic transducer consisted of a single unfocused piezoelectric crystal, 3 mm dia., which was mounted on the tip of a 5 cm long tungsten-epoxy stem. 10 MHz pulsed ultrasound was transmitted with a pulse repetition frequency of 20 KHz and received by the same crystal. For experimental convenience, the transducer was mounted at the end of a 0.45 m long, 5 mm ID stainless steel tube held by the probe mount described earlier. Thus, the transducer was lowered vertically into the flow field ($\theta = 0$).

The sample volume was approximately cylindrical, 0.45 mm in the direction of transmission and 3 mm in the transverse direction, with the equivalent volume of a sphere having 1.8 mm dia. For all the measurements in this study, the sample volume was located 3.5 transducer diameters away from the transducer face and hence was expected to be free from any transducer-induced artifacts. The PUDV used in this study was designed and built by C. J. Hartley of Baylor Medical College, Texas. The acoustic transducer was custom made by Etalon Corporation. The velocimeter output signal was passed through an external low pass filter (120 Hz cutoff) to an integrated data acquisition and processing microcomputer system (Data Precision, Data 6000). The microcomputer provided mean and RMS val-

ues of the detected signal from which the corresponding velocities were calculated.

The experimental procedure was tested for validity in a separate flow loop designed to study fully developed turbulence in pipe flow. Comparison of our results with the large body of published results using hot-film and laser-Doppler anemometry provided the required check. The comparison is shown in Figures 3 and 4. The relative turbulence intensity measurements at the centerline fell in the same range as many published results. Similarly, spectral measurements at a pipe Reynolds number of 5,900 followed the data of Garibini et al. (1982) very closely. These favorable comparisons provided a basis for confidence in the use of this PUDV to characterize the flow field of the experimental reactor. Additional details of the experimental procedure are available in Mehta (1985).

Mean and RMS velocities were measured in the reactor at several axial locations along the centerline and also at a few radial locations. Each measurement was repeated at least twice to check its reproducibility. The results were reproducible to within 5% for the mean and 15% for the RMS voltages with ±1 mv accuracy.

Four different experimental conditions were investigated corresponding to various placements of the turbulence generating screen and the "hairbrush" injector. In case 1, the honeycomb section was directly connected to the reactor pipe and the injector and the screen were not present. This allowed measurement of flow details from the downstream section of the honeycomb to the middle of the reactor pipe. In case 2, only the "hairbrush" injector was introduced and no screens were used. This was to assess the effect of the injector on the turbulence intensity level. In case 3, the largest screen (M_1) was placed 7 mm upstream of the injector, to evaluate the effect of this configuration on the turbulence, and in case 4, the same screen was placed 7 mm downstream from the injector. The presence of air bubbles in the system and their tendency to accumulate at the smaller screens (M_2 and M_3) prevented us from measuring the effect of smaller screens on the turbulence.

Results of flow field characterization

Turbulence measurements were conducted at a pipe Reynolds number of 3,400, the same as in the mixing-reaction experiments. The measured axial mean velocity at the reactor centerline is plotted as a function of axial distance in Figure 5a, and the corresponding relative turbulence intensity in Figure 5b.

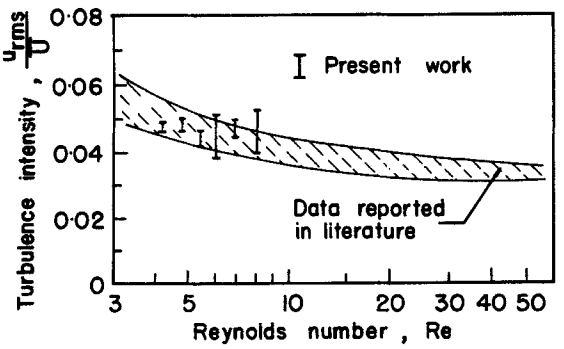

Figure 3. Centerline turbulence intensity measurements in pipe flow.
Hatched area corresponds to range of values reported in literature (Garibini et al., 1982)

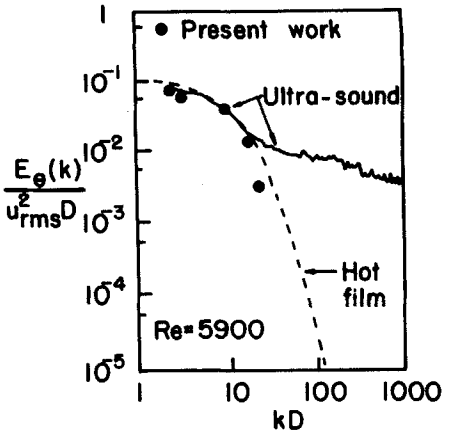

Figure 4. Normalized turbulence spectral densities at centerline of pipe flow.
— Ultrasound data ---- Hot film data of Garibini et al. (1982)

Zero on the abscissa of these figures corresponds to the plane of the injector needles. The mean velocities plotted in Figure 5a incorporate the correction due to the rise velocity of bubbles. Generally, this correction was less than 3%.

The centerline mean axial velocity profile shows how dramatically the flow speeds up during its passage through the contraction nozzle. The axial profile becomes relatively flat as the flow enters the reactor pipe although the velocity continues to increase gradually over the reactor length. Figure 5a reveals a 16% increase in the velocity from the entrance of the reactor to the exit. This applies to all the cases studied. Consequently, it is important to determine by how much the flow deviates from its desired one-dimensional character.

Velocity measurements were made at the reactor exit at several radial locations. Owing to limitations of the probe design, it was possible to access only the central 3 cm core of the reactor. In this region, the radial profile of mean axial velocity was found to be quite flat. The maximum deviation of the velocity from the mean axial centerline velocity was less than 3%. These results suggest that the mean velocity field was uniform in the central core over the entire length of the reactor. Since boundary layer growth, which causes acceleration of the core, is confined to the inaccessible annulus between the core and the pipe wall, the boundary layer thickness can only be estimated. Assuming a flat mean velocity profile in the central core and a linear mean velocity profile in the boundary layer with no slip at the wall, it is possible, by simple material balance, to calculate the boundary layer thickness that will cause a 16% rise in the core velocity at the exit. This calculation predicts a boundary layer thickness of 0.37 cm. The actual boundary layer would be thinner than this. Since the boundary layer is estimated to be thin and the measured mean velocity profile is flat, it is concluded that the reactor provides a nearly uniform mean axial velocity field along its length. This also confirms that we do not have a fully developed pipe flow and that the turbulence characteristics are determined by the turbulence generators (screens, injectors, straws, etc.).

The axial turbulence intensity profile depicted in Figure 5b can be used to make inferences about the homogeneity of the turbulent flow field. The reported turbulence intensities incorporate corrections for electrical noise as well as random noise associated with a variation in bubble rise velocity due to the dis-

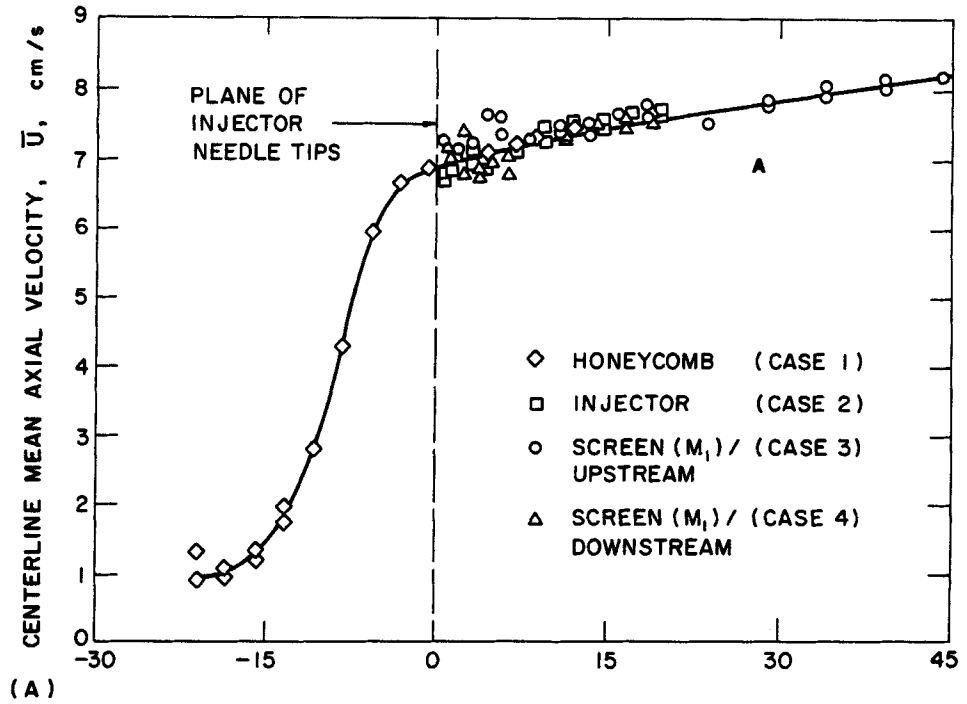

Figure 5a. Fluid mechanical measurements in reactor.
Centerline mean axial velocity.

tribution of bubble sizes. The corrections, which involve simply subtracting the noise levels from the measured signals, imply that the noise processes are uncorrelated with the true turbulence. No attempt is made here to justify this assumption since the turbulence intensity values are not used in any critical computations, but mainly as an indication of the homogeneity of the turbulence.

It is evident in Figure 5b that the turbulence intensity decays very rapidly to an asymptotic value of about 5% within 5 cm downstream of the injector. Nearly the same asymptotic level is

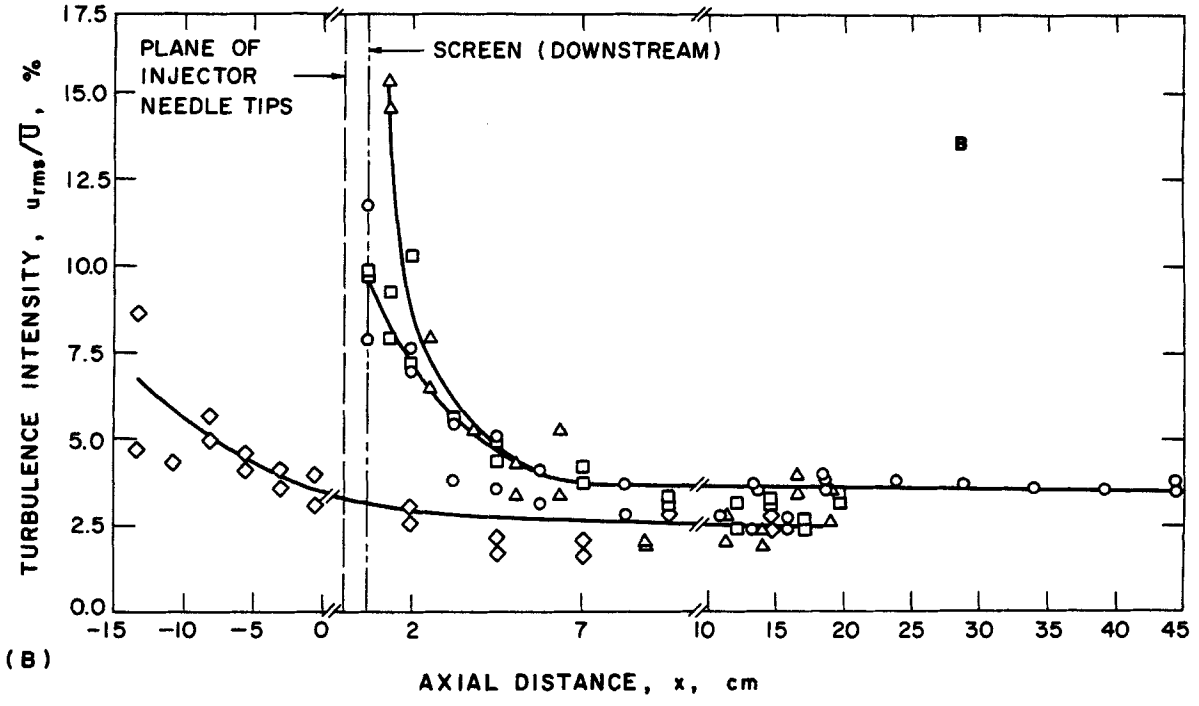

Figure 5b. Fluid mechanical measurements in reactor.
Centerline relative turbulence intensity
— smooth line through data points; symbols defined in Figure 5A

reached in all the cases studied, and this includes when screen M_1 is placed upstream or downstream of the injector. It is interesting to note that when the screen is placed upstream of the injector, it does not alter the intensity profile relative to the case where only the injector is used: compare the circles and squares in Figure 5b. In terms of micromixing, this indicates that placing a screen in the upstream location may not induce any additional mixing compared to that induced by the injector itself, at least in the case of the large screen, M_1. The highest turbulence level was measured within 2 cm of screen M_1 when it was in the downstream location: note the elevated positions of triangles in Figure 5a. This suggests that this configuration induces more intense micromixing than the other cases in the first 2 cm of the reactor. In any case, the first one-ninth (5 cm) of the reactor length has a varying turbulence level, while the last eight-ninths has an almost constant turbulence intensity. The radial profile of turbulence intensity measured at the reactor exit revealed a reasonable uniformity (less than 10% variation) over the cross section.

The foregoing discussion indicates that the reactor can be divided into two zones. The first zone corresponds to the initial 5 cm of the reactor, which has an elevated but varying turbulence level and hence enhanced but changing micromixing conditions. The second zone corresponds to the remaining 40 cm of the reactor, which is reasonably homogeneous for both the mean and fluctuating velocity fields. This zone has uniform micromixing conditions and is better suited to characterization by a single value of the micromixing parameter τ_m. Since the first zone covers only one-ninth of the reactor length, it is not expected to influence the reactions significantly except possibly when the screens are placed downstream of the injector.

Finally, it is useful to employ turbulence intensity values to estimate the micromixing time constant τ_m. τ_m has been given by Corrsin (1964) as

$$\tau_m \approx 0.5[4(L_s^2/\epsilon)^{1/3} + (\nu/\epsilon)^{1/2} \ln N_{sc}], \tag{4}$$

where L_S is the integral length scale of the concentration field, ϵ is the turbulent kinetic energy dissipation rate per unit mass, ν is the fluid kinematic viscosity, and N_{Sc} is the Schmidt number. ϵ may be estimated as

$$\epsilon \approx A u_{rms}^3 / l_e, \tag{5}$$

where the proportionality constant A is of order unity (Hinze, 1959), and l_e is the characteristic integral length scale of the velocity field corresponding to a characteristic transverse dimension of the flow field, that of the dominant turbulence generator. There are three turbulence generators in the present system: the honeycomb, injector, and screen. They all have similar characteristic dimensions: straw diameter = 0.6 cm, injector tube spacing = 0.65 cm, mesh spacing of M_1 = 0.42 cm. Any of these dimensions is adequate for the purpose of estimating τ_m. l_e = 0.42 cm is taken in the following estimate.

A reasonable estimate of L_s is 0.8 cm, which is the spacing of the injector needles. It is based on the fact that the jet streams, which carry the reactant B, expand and fill the reactor cross section about 2 cm downstream from the needles. Therefore, the expanded jet diameter, which equals the spacing of the injector needles, is an appropriate characteristic dimension of the concentration field. Similar arguments have been employed in the literature to estimate L_s (McKelvey et al., 1975).

Incorporating the above estimates for l_e and L_s along with a value of $\nu = 0.008$ cm^2/s (kinematic viscosity of water at 298 K), a typical liquid phase Schmidt number of 700, and a value of $u_{RMS} = 0.35$ cm/s, which is an average centerline RMS velocity over the length of the reactor, an estimate of τ_m is obtained: $\tau_m \approx$ 4.6 s. This is comparable to the time scale of the slow reaction (~1 s) and suggests that both reactions should be influenced by mixing in this reactor. Note that this is a reactor with extremely poor mixing. For comparison, the reactor of Vassilatos and Toor (1965) had a mixing time of 0.0082 s (Chang et al., 1986).

Mixing-reaction studies

The azo coupling of 1-naphthol (A) and diazotized sufanilic acid (B) in alkaline-buffered aqueous solution at room temperature leads to a distribution of two products, monoazo dye (R) and diazo dye (S). Since both R and S absorb visible light (A and B do not), absorption spectrophotometry (colorimetry) was employed to measure these concentrations. This technique is based on the Beer-Lambert law. Accordingly, when a monochromatic light beam (wavelength λ) of constant intensity I_o^λ passes through a sample of length l containing absorbing species i of concentration C_i, the resultant attenuated light intensity I^λ is given by

$$I^\lambda = I_o^\lambda \exp(-\epsilon_i^\lambda C_i l) \tag{6}$$

where ϵ_i^λ is the molar absorptivity of species i at wavelength λ. The Beer-Lambert law is assumed to hold for a stochastic concentration C_i, which can be decomposed into mean (overbar) and fluctuating (prime) components:

$$C_i = \overline{C_i} + C_i'. \tag{7}$$

In this case, the attenuated light intensity, I^λ, is also stochastic in nature. At the experimental concentration levels, R and S were assumed to absorb independently, leading to the following form of the Beer-Lambert law:

$$\ln\left(\frac{I_o^\lambda}{I^\lambda}\right) = \epsilon_R^\lambda l C_R + \epsilon_S^\lambda l C_S \tag{8}$$

Time-averaging Eq. 8 leads to

$$\overline{A^\lambda} = \overline{\ln\left(\frac{I_o^\lambda}{I^\lambda}\right)} = \epsilon_R^\lambda l \overline{C_R} + \epsilon_S^\lambda l \overline{C_S} \tag{9}$$

where $\overline{A^\lambda}$ is the mean absorbance of the reacting medium. Traditionally, $\overline{A^\lambda}$ is expressed in relation to a reference medium and hence

$$\overline{A^\lambda} = \overline{\ln\left(\frac{I_{ref}^\lambda}{I^\lambda}\right)} = \epsilon_R^\lambda l \overline{C_R} + \epsilon_S^\lambda l \overline{C_S} \tag{10}$$

where I_{ref}^λ is the intensity of light of initial intensity I_o^λ after its passage through a reference medium of path length l.

For local mean absorbance measurements, a colorimeter (Brinkman, model PC 801) was used in conjunction with a spe-

cially designed fiber-optic probe. The probe is shown schematically in Figure 6 and was fabricated according to our specifications by Fiberoptics Fabrications, Inc., MA. The transmitter fiber bundle had a 1 mm OD and was illuminated by the colorimeter light source at one end. The receiver fiber bundle, also 1 mm OD, was separated by a 1 mm gap from the end of the transmitter bundle, bottom of Figure 6, and carried the attenuated signal back to the colorimeter. Even though the gap size was small (dictated by high molar absorptivities of R and S), it was expected that boundary layer growth along the exposed fiber faces would have negligible effect on the measured absorbance values.

The colorimeter supplied phase-shifted, AC-modulated light from a tungsten filament lamp to the probe tip. The attenuated light beam from the receiver fiber bundle passed through an interference filter, which was mounted on a filter wheel, before impinging on the silicon photodetector. The filter wheel had six filters corresponding to wavelengths of 450, 470, 490, 520, 545, and 570 nm, with a 20 nm half-peak bandwidth for each filter. The photodetector generated a current directly proportional to light intensity, which was amplified and chopped by an electronic chopper that was synchronized with the light source but phase-shifted by 90°. This made the operation of the colorimeter more or less independent of the ambient light. The subsequent instrument circuitry essentially amplified the signal, ensured very good line stability, and provided an output voltage directly proportional to $\ln \overline{(I_o^\lambda/I^\lambda)}$:

$$\overline{V^\lambda} = k_p \ln \overline{(I_o^\lambda/I^\lambda)} \tag{11}$$

where k_p is the proportionality constant. The colorimeter was operated in the single-beam mode and hence required two separate measurements to obtain an absorbance value relative to buffer alkaline aqueous reference medium. When the fiber-optic probe was dipped into the reference solution, $\overline{V_{ref}^\lambda}$ was obtained where

$$\overline{V_{ref}^\lambda} = k_p \ln \overline{(I_o^\lambda/I_{ref}^\lambda)} \tag{12}$$

It was also estimated that the error introduced by equating $\ln \overline{(I_{ref}^\lambda/I^\lambda)}$ to $\overline{\ln (I_{ref}^\lambda/I^\lambda)}$ was less than 1% in the experimental range; see Mehta (1985) for details. The final form of the Beer-Lambert law used in this work was

$$\overline{\Delta V^\lambda} = k_R^\lambda \overline{C_R} + k_S^\lambda \overline{C_S} \tag{13}$$

where $\overline{\Delta V^\lambda} = \overline{V^\lambda} - \overline{V_{ref}^\lambda}$, $k_R^\lambda = k_p \epsilon_R^\lambda l$, and $k_S^\lambda = k_p \epsilon_S^\lambda l$. Both k_R^λ and k_S^λ are constants and were independently determined by calibration of the probe with known solutions of R and S. $\overline{\Delta V^\lambda}$ values were measured at 450, 470, 490, 520, and 545 nm at each location in the reactor. Substitution of these values into Eq. 13, along with the corresponding calibration constants k_R^λ and k_S^λ resulted in a set of five equations involving only two unknowns, $\overline{C_R}$ and $\overline{C_S}$. A standard linear regression routine (MINITAB) was used to find the best-fit values of $\overline{C_R}$ and $\overline{C_S}$. These values are termed the experimental values in this paper. Under reactor operating conditions the standard deviations of these regressed values averaged 10% and 17% for $\overline{C_R}$ and $\overline{C_S}$, respectively.

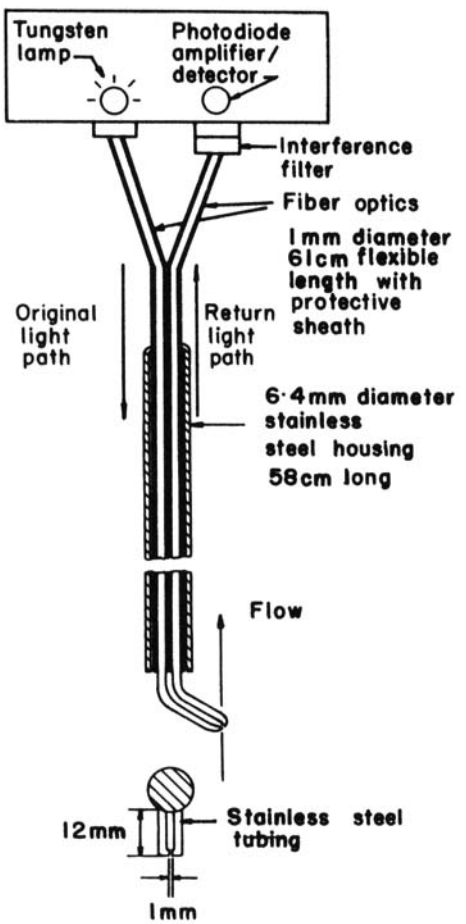

Figure 6. Fiber-optic probe.

Chemicals

Distilled water at room temperature was used as the working fluid; sodium carbonate and sodium bicarbonate ("Baker-analyzed," J. T. Baker and Co., NJ) were used as buffer salts. Recrystallized 1 naphthol ("Certified," Fisher Scientific Co., NJ) and diazotized sulfanilic acid ("Purum p.a.," Fluka Chemical Corp., NY)—reactants A and B—were both reagent grade pure. The latter was available as a moist paste from the manufacturer because of its explosive nature. The actual diazotized sulfanilic acid content of the paste was supplied by the manufacturer as actual lot analysis. Typically the paste contained about 30% water.

A standard solution of R in alkaline buffered water of pH 10.00 ± 0.02 was prepared by adding a known weight of commercially available pure R powder ("Standard Fluka," Fluka Chemical Corp., NY). The standard solution of S was prepared by carrying out the second azo coupling reaction $R + B \rightarrow S$ in a beaker under conditions of pH and ionic strength *simulating* reactor conditions.

Calibration of fiber-optic probe

Five solutions of R and S, of various concentrations in the range 0.07 to 0.35 mol/m^3 were prepared by suitably diluting the standard solution with an alkaline buffer of $Na_2CO_3/NaHCO_3$ (pH 10.00) at room temperature. $\overline{\Delta V^\lambda}$ values were mea-

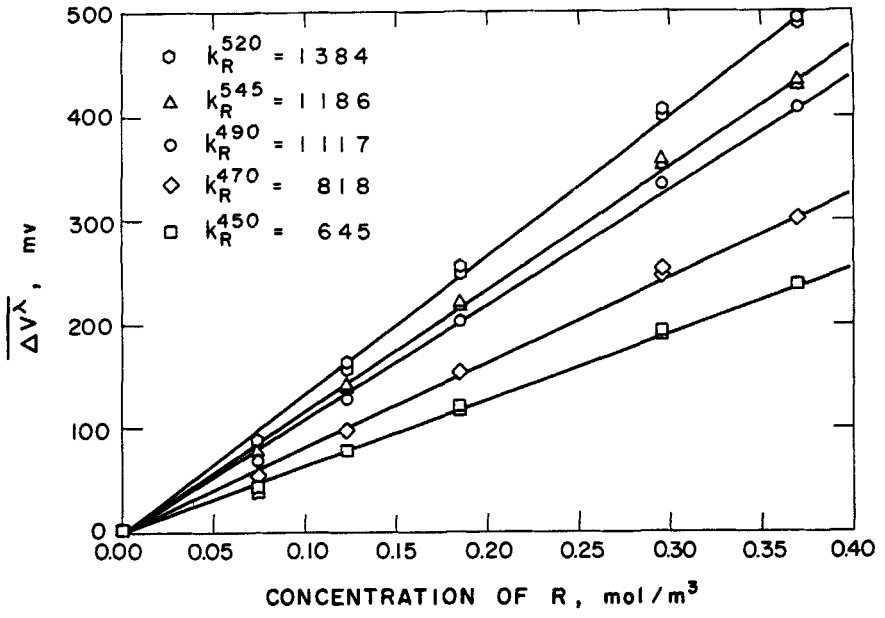

Figure 7. Fiber-optic probe calibration data for monoazo dye *R*.
Slopes have units of mv/mol/m³

sured at five wavelengths in each of those solutions. At each wavelength, measured $\overline{\Delta V^\lambda}$ values were regressed against the known concentrations using the standard linear regression routine (MINITAB) and k_R^λ and k_S^λ were obtained as the best-fit values for the equations:

$$\overline{\Delta V^\lambda} = k_R^\lambda \overline{C_R} \text{ and } \overline{\Delta V^\lambda} = k_S^\lambda \overline{C_S} \qquad (14)$$

Typical calibration are displayed in Figures 7 and 8.

The method used to analyze experimental data was also tested with solutions containing known concentrations of both R and S. The concentration range was typical of the range expected to exist in the reactor under experimental conditions. The measured concentrations were found to be within 12% of the actual concentrations. This was considered satisfactory in view of the low concentration levels. The method was found to be too inaccurate when C_S was more than 15 times lower than C_R. Nevertheless, the experimental data could be reasonably analyzed in such cases by ignoring the presence of S altogether and finding the best-fit value for C_R only. This approximate method of analysis yielded an agreement to within 15% of the actual value of C_R. As will be discussed later, this approximate analysis

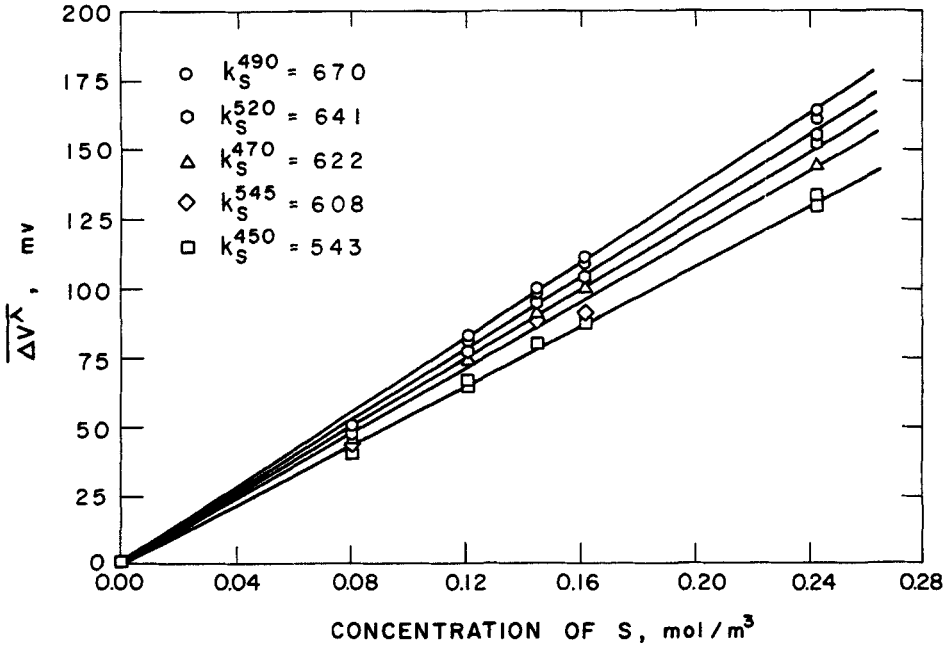

Figure 8. Fiber-optic probe calibration data for diazo dye *S*.
Slopes have units of mv/mol/m³

was employed to measure the concentration of R in experiments with a low ratio of B to A in the feed.

Reactor experiments

The primary feedstream in the mixing-reaction experiments contained 1-naphthol (A) in an aqueous buffer solution of $Na_2CO_3/NaHCO_3$ (pH 10.00 ±0.02). The same amounts of distilled water and 1-naphthol were used for each experiment. Thus, the unmixed feed concentration C_{AO} was always about 0.3 mol/m^3. The exact value was determined by measuring the UV absorbance of the solution at 245 nm. The secondary stream was a relatively concentrated solution (10–30 mol/m3) of diazotized sulfanilic acid in water. The actual lot analysis supplied by the manufacturer was used to calculate the amount of paste required to prepare a solution of required concentration.

The details of the experimental procedure may be found in Mehta (1985). The actual duration of a mixing-reaction experiment was about 20 min, although preparation required 24 h. Briefly, 1-naphthol was dissolved into the distilled water by stirring the contents of the 0.21 m^3 tank overnight. The buffer salts were added only 30 min prior to the reactor run. The salts dissolved rapidly and brought the pH to 10.00 ±0.02, corresponding to an approximate ionic strength of 10 g ion/m^3. The pH was monitored with a standard pH meter (Digital Ionalyzer/501, Orion Corp., MA). Just before start-up of the reactor, a fresh solution of diazotized sulfanilic acid was prepared in a separate beaker. The mainstream rotameter and the secondary stream metering pump were calibrated for each run with a measuring cylinder and a stop watch. The feedstreams were approximately at room temperature and always remained steady throughout the experiment. During each experiment, a small beaker of the feed solution of A was kept at hand for use as the reference solution. The fiber-optic probe was dipped into this beaker to measure the reference voltage, V_{ref}, at each wavelength, λ. The probe was then lowered into the reactor, the pumps were turned on at preset speeds, and data collection was begun. Usually, it required a 3 s real-time record of the signal to obtain a statistically stable value of $\overline{V^{\lambda}}$. For each λ, six different axial positions were interrogated by the probe. After measuring at the sixth location, the probe was again dipped into the reference solution to check for any baseline drift. An arithmetic mean of the two $\overline{V^{\lambda}_{ref}}$ values was used in the calculation of $\Delta\overline{V^{\lambda}}$. The filter wheel on the colorimeter was then set to a new λ value and another axial traverse was obtained. Three effluent samples were also collected at approximately 5 min intervals and analyzed at the end of the experiment. This provided a check on the steady operation of the reactor.

The effect of feed stoichiometric ratio β (ratio of B to A) on the product distribution was studied at a fixed mixing intensity in 22 mixing reaction experiments carried out over a period of three months. Three different stoichiometries (β = 0.39, 1.00, and 1.54) were investigated by varying the feed concentration of B. In general, all the experimental conditions were repeated at least three times to check for reproducibility. In some cases, more than three runs were made to obtain data from the region very close to the injector to the farthest end of the reactor.

Kinetics

To clearly interpret mixing-reaction experiments, it is important to have reliable chemical kinetic information available. Kozicki (1980), Bourne et al. (1981), and Baldyga and Bourne (1984) have reported the results of stopped-flow kinetic experiments for the reactions employed in the present work. Both of the azo coupling reactions are reported to be irreversible and second order in concentration dependence so that

$$-r_A = k_1 C_A C_B \tag{15}$$

and

$$r_S = k_2 C_R C_B$$

Bourne et al. (1981) reported the following values of the rate constants at pH 10.00 and 298 K: $k_1 = 7.3 \times 10^3$ m^3/mol/s, and $k_2 = 3.5$ m^3/mol/s. Since k_1 is three orders of magnitude higher than k_2, theoretical model predictions are found to be insensitive to modest variations in k_1 (Chang et al., 1986). Therefore, this value of k_1 will be used in model simulations for all experiments. The temperature dependence of k_2 was reported by Kozicki (1980):

$$k_2 = 1.93 \times 10^9 \exp(-5{,}989/T) \text{ m}^3/\text{mol/s} \tag{16}$$

Baldyga and Bourne (1984) however, used the following expression

$$k_2 = 1.11 \times 10^6 \exp(-3{,}957/T) \text{ m}^3/\text{mol/s} \tag{17}$$

These expressions differ by a factor of about two at room temperature. In view of the ambiguity in k_2, we will use Eq. 16 to compare model predictions with the data, but will also show variations in the predictions associated with the use of Eq. 17.

Modeling

In a previous work (Chang et al., 1986) we evaluated five models of mixing and chemical reaction having an analogy with isotropic turbulence through numerical simulations of competing reactions in a plug flow reactor with unmixed feedstreams. We found wide variations among the models in selectivity prediction, and that provided the major impetus for the present work. Among the five models with a turbulence analogy, the three-environment (3E) model of Ritchie and Tobgy (1979) was considered to be grossly inadequate for selectivity predictions. Failure of the 3E model was attributed to the lack of "rich" and "lean" reacting regions in the model structure. An evaluation of the remaining four models by comparison of their predictions with the experimental data in the present work might be attempted. Unfortunately, for the experimental conditions, which involve highly unequal reactant stream flow rates, the slab-diffusion (SD) model of Mao and Toor (1970) does not possess a turbulence analogy, and the coalescence-redispersion (CRD) model of Curl (1963) requires an exorbitant amount of computer time. Because of the high flow-rate inequality, the axial concentration profiles predicted by the CRD model are very sensitive to the number of eddies chosen for the simulation, although the exit concentrations are fairly insensitive. For meaningful prediction of profiles, either the number of eddies has to be increased by an order of magnitude (from 100 to 1,000) or the simulation has to be conducted several times, each with a different sequence of random numbers, and the results

ensemble-averaged. Both of these alternatives are economically prohibitive. However, previous simulations for equal flow rates (Chang et al. 1986) did show that the CRD and the four-environment (4E) model of Mehta and Tarbell (1983) give similar predictions and that the interaction by exchange with the mean (IEM) model of Villermaux and Devillon (1972) and SD model also give similar predictions. In the following, therefore, the 4E and IEM models are used to compare model predictions with the experimental data.

Results and Discussion

The results of the mixing-reaction experiments are displayed in Figures 9–11. The ordinate of each figure is concentration normalized by the (mixed) feed concentration of B, $\overline{C_{BO}}$. $\overline{C_{BO}}$ is given by $\overline{C_{BO}} = C_{BO}Q_B/(Q_A + Q_B)$. The abscissa is the axial distance from the injector needle tips. The squares represent the arithmetic mean of experimental data obtained at each location, and the vertical error bars represent the range over which the experimental results varied in all experiments (typically three). The error bars are not based on statistical measures (e.g., standard deviation) since experiments were repeated only three times. The smooth curves are the predictions of various models: maximum mixedness (MM), IEM, and 4E. The curves labeled 4E and 4E′ are for predictions with k_2 given by Eqs. 16 and 17, respectively. Predictions for the MM and IEM models are based on the use of Eq. 16 for k_2. The error bars result principally from the relatively low signal-to-noise ratio inherent in the present absorbance measurement system. It should also be emphasized that the experimental concentration levels are very low and are intrinsically difficult to measure accurately on-line. The other suspect source of error is the low flow rate of the highly concentrated B stream, Figure 2. However, a maximum error in the flow rate of B is estimated from calibrations to be ± 0.06 mL/s, and can cause only a ±3% variation in the mixed feed concentration of B.

The input parameters for the models were the feed flow rates Q_A and Q_B; the unmixed feed concentrations C_{AO} and C_{BO}; the operating temperature T_{avg}; the mean axial velocity $\bar{U}$; and the micromixing time τ_m. Since each experiment was repeated at least three times, the corresponding values of the input parameters were taken as arithmetic averages of the actual conditions for all runs at the same nominal operating conditions. A constant value of $\bar{U} = 7.6$ cm/s was used as input for all the simulations.

The only adjustable parameter in the models is τ_m. The actual model parameters—R_S for the 4E and h for the IEM—are related to τ_m through the turbulence analogy: $R_S = 2h = 1/\tau_m$ (Tarbell and Mehta, 1986). The models may be used to fit the experimental data by varying τ_m, and in this work an "eyeball" fit was considered adequate to determine the "best" value of τ_m rather than a more sophisticated statistical method.

Ordinarily, both models would have been fitted to the data independently and then evaluated for their relative success. However, in the present study the IEM model was unable to simultaneously match the experimental profiles of both R and S, regardless of the value of τ_m or k_2 used, for $\beta > 1$. A reasonable match of the IEM model predictions for $\overline{C_R}$ always led to very poor predictions of $\overline{C_S}$. In fact, $\overline{C_S}$ profiles could not be matched at all unless an arbitrarily higher value of k_2 was used. For $\beta = 0.39$, when virtually no S was produced, reasonably good predictions were possible with the IEM model. As a consequence of the overall inability of the IEM model to make reasonable predictions, the question of model evaluation was narrowed down to considering the ability of only the 4E model to predict the experimental data. In Figures 9–11, the predictions of the IEM and maximum mixedness models are displayed only to highlight the differences between them and the 4E model predictions. In addition, the 4E′ model predictions for k_2 given by Eq. 17 are also displayed to show that conclusions remain unchanged for either of the k_2 values. A significantly better fit of the 4E′ model could be obtained by increasing τ_m.

Figure 9 shows the results of experiments with screen M_1 in its upstream position. This case was discussed previously from a fluid mechanical viewpoint (case 4) and was found to be most suited for a model evaluation because the turbulence field was most homogeneous. For the results shown in Figure 9, the stoichiometric ratio of the feed, β, was very low (0.39). Because of the limited B present and the fact that the first coupling ($A + B \rightarrow R$) is three orders of magnitude faster than the second ($R + B \rightarrow S$), the concentration of S is expected to be nearly zero. This is essentially a single-reaction case and we do not expect to be able to discriminate between models here; Chang et al. (1986). Because the S concentration was expected to be near zero in this case, the experimentally observed absorbance was attributed entirely to R and the approximate method of concentration calculation described previously was used. The reaction results displayed in Figure 9 indicate that $\tau_m = 2$ s is a good estimate of the micromixing time for the 4E model. This value is in accord with the previous fluid mechanical results ($\tau_m \sim 4.5$ s). With $\tau_m = 2$ s, the IEM model also provides a reasonably good fit to the data. In fact, the fit of the IEM model could be improved if a somewhat lower value of τ_m were chosen, but this leads to poorer predictions for higher values of β. In effect, this operating condition ($\beta = 0.39$) has served as a fast single-reaction calibration case allowing us to fix the value of τ_m.

The results of experiments with an equimolar feed ($\beta = 1.0$), but with an identical screen-injector configuration are displayed in Figure 10. Although there is scatter in the experimental data, particularly for S close to the injector (due to very low values of C_S), the 4E model predictions are in satisfactory agreement

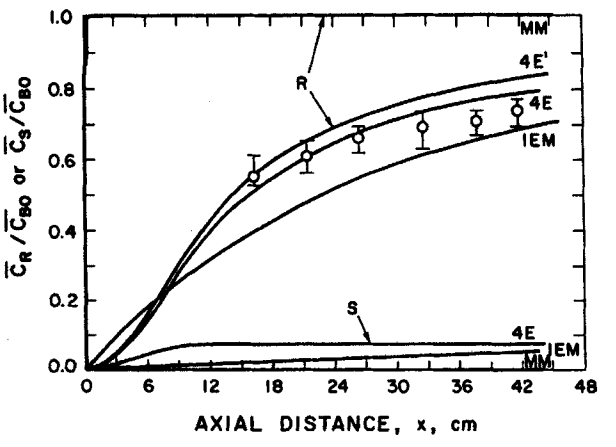

Figure 9. Mean concentration profiles for products.
$\beta = 0.39$; screen M_1 upstream of injector; $\tau_m = 2.0$ s
4E, 4E′, Predictions of 4E model with k_2 given by Eqs. 16 and 17, respectively
MM, Maximum mixedness prediction, O data points
$Q_A(Q_B) = 135\ (2.13)$ cm³/s, $C_{AO}(C_{BO}) = 0.3\ (7.45)$ mol/m³

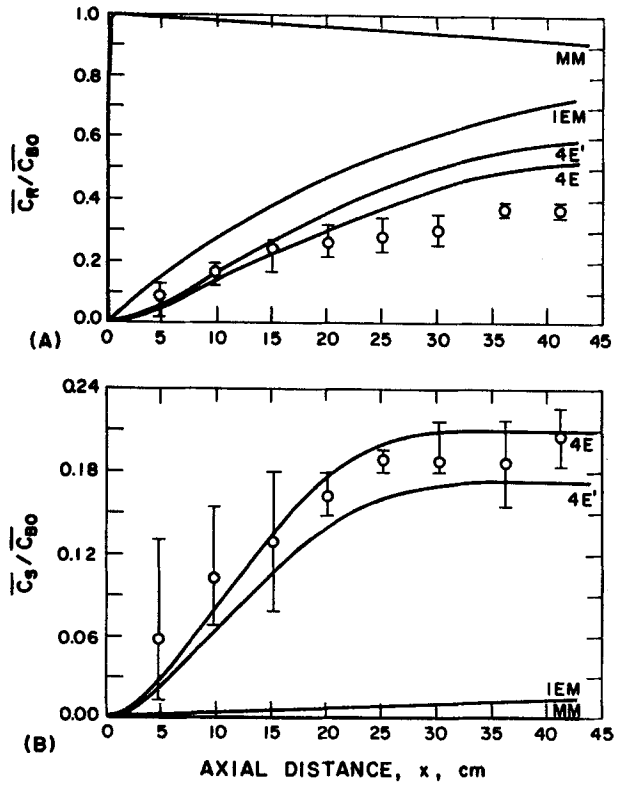

Figure 10. Mean concentration profiles for products.
β = 1.0; screen M_1 upstream of injector; τ_m = 2.0 s
A. Profile of monoazo dye
B. Profile of diazo dye
$Q_A(Q_B)$ = 131 (1.31) cm³/s, $C_{AO}(C_{BO})$ = 0.3 (30) mol/m³

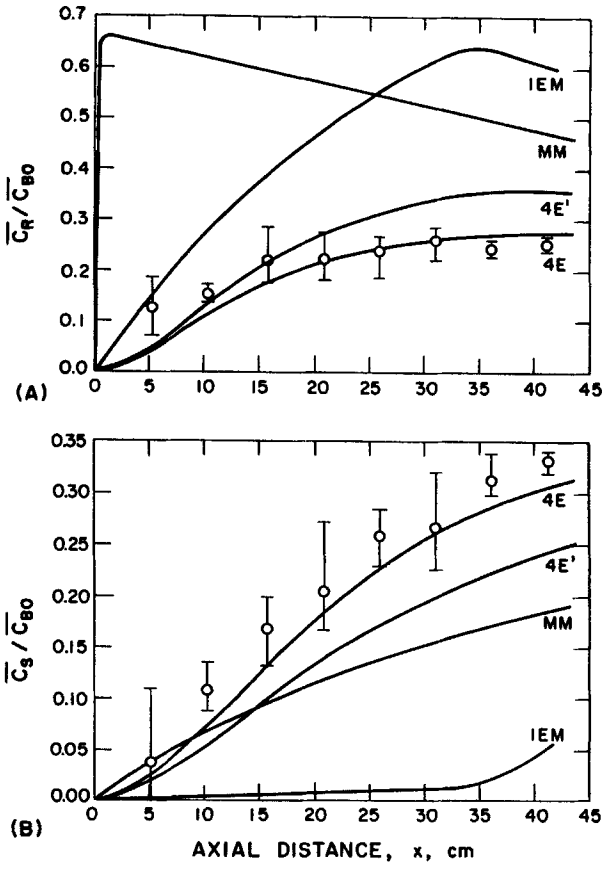

Figure 11. Mean concentration profiles for products.
β = 1.53; screens M_1, M_2, M_3 upstream of injector; τ_m = 2.0 s
A. Profile of monoazo dye
B. Profile of diazo dye
$Q_A(Q_B)$ = 136 (2.12) cm³/s, $C_{AO}(C_{BO})$ = 0.3 (7.45) mol/m³

with the data, again for a value of τ_m = 2 s. Note that the hydrodynamic conditions in this case (β = 1.0) are identical to those of the previous case (β = 0.39) and thus τ_m should be the same. The failure of the IEM model (τ_m = 2 s) is also evident in this figure, particularly in prediction of the S concentration.

The data for a still higher stoichiometric ratio (β = 1.53) with the same screen-injector arrangement is shown in Figure 11. Again, the 4E model compares favorably with the experimental data for a value of τ_m = 2. It should be pointed out that in two of the experiments that contribute to the results of Figure 11, finer screens (M_2 and M_3) were employed in the upstream position, and yet no change in the R and S concentration profiles were observed. This is consistent with our fluid mechanical measurements, which showed that when a screen is placed upstream of the injector, its effect on the turbulence intensity is indistinguishable from that of the injector itself. The IEM model greatly overpredicts the concentration of R and predicts negligible concentration of S, which is in clear contrast with the experimental measurements.

In view of Figures 9–11, it is clear that the effect of mixing on selectivity (concentrations of R and S) is very large. This is reflected in the large differences between the experimental data and the maximum mixedness model predictions. Both turbulent mixing models—4E and IEM—predict a large effect on the concentration of R, but only the 4E model is able to predict the S concentration data accurately. It is concluded from these comparisons with experiments that the 4E model is able to simulate the effect of varying feed stoichiometry (β) on the product distribution under constant mixing conditions (constant τ_m) quite well.

Concluding Remarks

Our experimental results provide direct evidence that under appropriate conditions, models of mixing and chemical reaction that are indistinguishable in their ability to predict single-reaction data may predict grossly different product distributions for competing reactions. The required condition for model discrimination is that the mixing time be comparable to or greater than the slowest reaction time. In other words, both reactions should be mixing-limited.

The present experimental data provide a firm basis for evaluating models of mixing and reaction. To date we have found that the 4E model is able to simulate the experimental behavior at all operating conditions, but the IEM model is not. The SD model simply cannot handle unequal flow rates and cannot be used to simulate the present data. Similarly, the CRD model cannot be tested due to prohibitive requirements for computer time. The failure of the IEM and, as shown earlier (Chang et al., 1986), 3E models and the relative success of the 4E model underscores the importance of certain structural features such as the existence of "rich" and "lean" reacting regions and the presence of regions of total segregation.

The 4E model has many attractive features, such as:

- Applicability to arbitrary feed flow rates, arbitrary feed residence time distributions, and arbitrarily complex chemical kinetics
- Mathematical simplicity (ODE's) and modest computational requirements
- The fact that its model parameter can be reliably estimated *a priori* or measured from fast single-reaction experiments. Thus, the 4E model appears to be a very useful chemical reactor model for homogeneous systems.

Finally, we are hopeful that the experimental data provided in this paper will prove useful to others in the evaluation of models for mixing and chemical reaction in turbulent flows.

Note Added in Review

When the present manuscript was being reviewed, a new publication by Bourne et al. (1985) appeared in which the kinetics of the present reaction system were further revised. According to this new revision, the reactions should be represented in general by

$$A + B \begin{matrix} \nearrow p\text{—}R + B \searrow \\ \searrow O\text{—}R + B \nearrow \end{matrix} S + B \begin{matrix} \nearrow \mathrm{P_1} \\ \searrow \mathrm{P_2} \end{matrix} \qquad (18)$$

where p—R and O—R denote R coupled in para and ortho positions, respectively. The paper, however, suggests that if $\overline{C_S/C_{BO}}$ is less than 20%, the degradation of disazo dye S to P_1 and P_2 can be neglected. In that event, the reactions are well represented by the parallel-consecutive scheme:

$$A + B \xrightarrow[1]{k_1} R$$

$$R + B \xrightarrow[1]{k_2} S$$

with

$$5.3 \times 10^3\ \mathrm{m^3/mol/s} < k_1 < 1.1 \times 10^4\ \mathrm{m^3/mol/s} \qquad (20)$$

at $T = 293$ K and pH = 10.0, and

$$k_2 = 3.338 \times 10^6 \exp(-4{,}257/T)\ \mathrm{m^3/mol/s} \qquad (21)$$

We would like to make a few comments about the present work in light of this new information. First, in most of our experiments $\overline{C_S/C_{BO}}$ is indeed less than 20%, and hence degradation of S can be neglected. Even when $\overline{C_S/C_{BO}} = 0.3$ (the maximum value observed in our experiments), Bourne et al. (1985) recorded an error of only 8% in the overall mass balance due to degradation of S. This is within the accuracy of our measurements and does not affect our results. Second, the new rate constants, although different than those employed in our modeling, do not warrant new simulations. k_1 is still three orders of magnitude larger than k_2 and the results are insensitive to the exact value of k_1. More critically, the new k_2 (Eq. 21) lies between the previous two k_2 values (Eqs. 16 and 17), and hence predictions based on the new k_2 value would fall in the region bounded by the 4E and 4E′ curves in Figures 9–11. Thus, our analysis, model comparisons, and conclusions remain unchanged in light of the new kinetic information.

Acknowledgment

This work was supported by the Naval Sea Systems Command and the Applied Research Laboratory Exploratory and Foundational Research Program of The Pennsylvania State University.

Notation

A = dimensionless constant, Eq. 5
A = absorbance
A = 1-Naphthol
B = diazotized sulfanilic acid
C_j = concentration of species j
CRD = Coalescence-redispersion model
D = diameter
E = one-dimensional turbulence spectral density
f = frequency
h = micromixing parameter of IEM model
I = intensity of light
I_S = intensity of segregation
IEM = Interaction by exchange with mean model
I.D. = Inner diameter
k, k_1, k_2 = rate constants
k_j = fiber-optic probe calibration constant for species j at wavelength λ
k_p = proportionality constant
L = length
l = optical path length
l_e = integral length scale of turbulence field
L.E. = leaving environment
L_S = scalar macroscale
M = concentration, mol/m^3
MM = Maximum mixedness model
M_1, M_2, M_3 = screens
N_{Sc} = Schmidt number
PFR = Plug flow reactor
PRF = pulse repetition frequency
PUDV = Pulsed Ultrasound Doppler Velocimeter
Q = flow rate
r = reaction rate
R = monazo dye
Re = Reynolds number
R_s = micromixing parameter of four-environment model
RTD = Residence time distribution
r.m.s. = Root-mean-square value
SD = Slab diffusion model
S = diazo dye
S = solidity
T = temperature
u = fluctuating velocity
u = velocity of moving object, Eq. 2
u_s = speed of sound
U = mean velocity
V = voltage output
x, x' = axial distance

Greek letter

β = feed stoichiometric ratio $Q_B C_{BO}/Q_A C_{AO}$
Δ = difference
ϵ = turbulent energy dissipation rate per unit mass
θ = angle
λ = wavelength
σ^2 = variance of concentration distribution
ν = kinematic viscosity
τ = mean residence time
τ_m = micromixing time
ω = angular frequency

Subscript

A, B, R, S = chemical species
Cr = critical
d = wire diameter based
d = Doppler shift
M = mesh-size based
O = feed condition

Superscript

λ = wavelength

Specific symbols

(overbar) = Time-averaged or flow-averaged value
(prime) = fluctuating part
3E = three-environment model
4E = four-environment model

Literature cited

Baldyga, J., and J. R. Bourne, "A Fluid Mechanical Approach to Turbulent Mixing and Chemical Reaction. III," *Chem. Eng. Commun.*, **28**, 259 (1984).

Bourne, J. R., "The Characterization of Micromixing Using Fast Multiple Reactions," *Chem. Eng. Commun.*, **16**, 79 (1982).

Bourne, J. R., C. Hilber, and G. Tovstiga, "Kinetics of the Azo Coupling Reactions between 1-Napthol and Diazotized Sulphanilic Acid," *Chem. Eng. Commun.*, **37**, 293 (1985).

Bourne, J. R., F. Kozicki, and P. Rys, "Mixing and Fast Chemical Reaction. I: Test Reactions to Determine Segregation," *Chem. Eng. Sci.*, **36**, 1643 (1981).

Brodkey, R. S., "Fundamentals of Turbulent Motion, Mixing and Kinetics," *Chem. Eng. Commun.*, **8**, 1 (1981).

Brodkey, R. S., and J. Lewalle, "Reactor Selectivity Based on First-Order Closures of the Turbulent Concentration Equations," *AIChE J.*, **31**, 111 (1985).

Chang, L.-J., R. V. Mehta, and J. M. Tarbell, "Evaluation of Models of Mixing and Chemical Reaction with a Turbulence Analogy," *Chem. Eng. Commun.*, **42**, 139 (1986).

Corrsin, S., "The Isotropic Turbulent Mixer. II: Arbitrary Schmidt Number," *AIChE J.*, **10**, 870 (1964).

Curl, R. L., "Dispersed Phase Mixing. I: Theory and Effects in Simple Reactors," *AIChE J.*, **9**, 175 (1963).

Garibini, J. L., F. K. Forster, and J. E. Jorgensen, "Measurement of Fluid Turbulence Based on Pulsed Ultrasound Technique. 2: Experimental Investigation," *J. Fluid Mech.*, **118**, 471 (1982).

Garside, J., "Industrial Crystallization from Solution," *Chem. Eng. Sci.*, **40**, 3 (1985).

Hill, J. C., "Models for Turbulent Transport Processes," *Chem. Eng. Ed.*, **13**, 34 (1979).

Hinze, J. O., *Turbulence*, 1st ed., McGraw-Hill, New York (1959).

Jorgensen, J. E., D. N. Campau, and D. W. Baker, "Physical Characteristics and Mathematical Modeling of the Pulsed Ultrasonic Flowmeter," *Med. Biol. Eng.*, **11**, 404 (1973).

Keeler, R. N., "Mixing and Chemical Reactions in Turbulent Flow Reactors," Ph.D. Thesis, Univ. California, Berkeley (1964).

Kozicki, F. R. "Selektivitat Mischungsmaskierter Reaktionen in Ruhrkesseln," Ph.D. Thesis, ETH, Zurich, Switzerland (1980).

Li, K. T., and H. L. Toor, "Turbulent Reactive Mixing with a Series-Parallel Reaction: Effect of Mixing on Yield," *AIChE J.*, (1986).

Mao, K. W., and H. L. Toor, "A Diffusion Model for Reactions with Turbulent Mixing," *AIChE J.*, **16**, 49 (1970).

McKelvey, K. N., H. N. Yieh, S. Zakanycz, and R. S. Brodkey, "Turbulent Motion, Mixing, and Kinetics in a Chemical Reactor Configuration," *AIChE J.*, **21**, 1165 (1975).

Mehta, R. V., "Experimental Study of Turbulent Mixing and Selectivity of Competing Reactions," Ph.D. Thesis, Penn. State Univ. (1985).

Mehta, R. V., and J. M. Tarbell, "Four-Environment Model of Mixing and Chemical Reaction. I," *AIChE J.*, **29**, 320 (1983).

Patterson, G. K., "Closure Approximations for Complex Multiple Reactions," *2nd Shear Turbulence Symp.*, London, (July, 1979).

———, "Application of Turbulence Fundamentals to Reactor Modeling and Scale-up," *Chem. Eng. Commun.*, **8**, 25 (1981).

Pratt, D. T., "Mixing and Chemical Reaction in Continuous Combustion," *Prog. Energy Combust. Sci.*, **1**, 73 (1976).

Ritchie, B. W., and A. H. Tobgy, "A Three-Environment Micromixing Model for Chemical Reactors with Arbitrary Separate Feedstreams," *Chem. Eng. J.*, **17**, 173 (1979).

Tan Atichat, J., H. M. Nagib, and R. I. Loehrke, "Interaction of Free Stream Turbulence with Screens and Grids: A Balance Between Turbulent Scales," *J. Fluid Mech.*, **114**, 501 (1982).

Tarbell, J. M., and R. V. Mehta, "Mechanistic Models of Mixing and Chemical Reaction with a Turbulence Analogy," *Physicochem. Hydrodynam.*, **7**, 17 (1986).

Tarbell, J. M., J. P. Gunshinan, O. B. Geselowitz, G. Rosenberg, K. K. Shung, and W. S. Pierce, "Pulsed Ultrasound Doppler Velocity Measurements Inside a Left Ventricular Assist Device," *J. Biomech. Eng.*, **108**, 232 (1986).

van der Molen, T. J., A. Koenen, H. H. J. Oosterwijk, and H. Th. van der Bend, "Effect of Process Conditions on Light-off Temperature and Consumption of Sixteen Initiators, as Determined from High-Pressure Radical Polymerization of Ethylene," *Ing. Chim. Ital.*, **18**, 7 (1982).

Vassilatos, G., and H. L. Toor. "Second-order Chemical Reactions in a Nonhomogeneous Turbulent Fluid," *AIChE J.*, **11**, 666 (1965).

Villermaux, J., "Mixing in Chemical Reactors," *ACS Symp. Ser. No. 226*, 135 (1983).

Villermaux, J., and J. C. Devillon. "Representation de la Coalescence et de la redisperison des domaines de segregation dans un fluide par un modele dinteraction phenomenologique," *2nd Symp. Chem. Reac. Eng.*, B-1-13 (1972).

Manuscript received July 29, 1986, and revision received Dec. 23, 1986.